Foam Engineering

Fundamentals and Applications

Edited by

Paul Stevenson

Department of Chemical and Materials Engineering,
Faculty of Engineering, University of Auckland, New Zealand

WILEY-BLACKWELL

A John Wiley & Sons, Ltd., Publication

This edition first published 2012

Registered Office
John Wiley & Sons, Ltd, The Atrium, Southern Gate, Chichester, West Sussex, PO19 8SQ, United Kingdom

Library of Congress Cataloging-in-Publication Data

Foam engineering : fundamentals and applications / [edited by] Paul Stevenson. – 1st ed.
p. cm.
Includes bibliographical references and index.
ISBN 978-0-470-66080-5 (hardback)
1. Foam. 2. Foam–Industrial applications. 3. Foam–Technological innovations. 4. Foamed materials.
I. Stevenson, Paul, 1973–
QD549.F59 2012
620.1–dc23

2011037211

A catalogue record for this book is available from the British Library.

Print ISBN: 9780470660805

Set in 10/12pt Times by SPi Publisher Services, Pondicherry, India
Printed and bound in Singapore by Markono Print Media Pte Ltd

6

Foam Rheology

Nikolai D. Denkov, Slavka S. Tcholakova, Reinhard Höhler and Sylvie Cohen-Addad

6.1 Introduction

Rheological properties of foams, such as elasticity, plasticity, and viscosity, play a major role in foam production, transportation, and applications [1–8]. Obvious examples are foam extrusion through nozzles and slits (used in cosmetic and food applications, and in plastic foam production), transportation through pipes (e.g. for compartment cleaning in nuclear plants and in foam-aided natural gas production), flow through porous media (in enhanced oil recovery), foam perception in personal and home care applications (shaving and styling foams, facial cleansers, shampoos), and many others – see Chapter 18 in this book for further examples.

Understanding foam rheology is a challenging scientific problem, mainly due to the complexity of the interactions and processes involved [4–14]. By definition, foams are bubble dispersions with gas volume fraction, $\Phi = V_{gas}/V_{foam}$, higher than that of closely packed spheres ($\Phi_{CP} \approx 0.64$ for disordered foam). Therefore, neighbouring bubbles are squeezed against each other and separated by thin films and Plateau borders, whose liquid–gas interfaces are stabilized by surfactants, proteins, polymers or solid particles [1–4]. If foam is subjected to a small shear stress, it deforms like a soft solid. This response can be characterized by visco-elastic moduli [2, 4, 8, 12]. For applied stresses beyond a threshold, called 'yield stress', visco-plastic flow sets in. In this regime, foams behave like shear-thinning fluids, which means that their effective viscosity is a decreasing function of shear rate [4, 7, 8, 12, 14]. Additional rheological phenomena arise at the contact between foams and confining solid walls: If the surface of the solid wall is smooth on the scale of the bubble

Foam Engineering: Fundamentals and Applications, First Edition. Edited by Paul Stevenson.

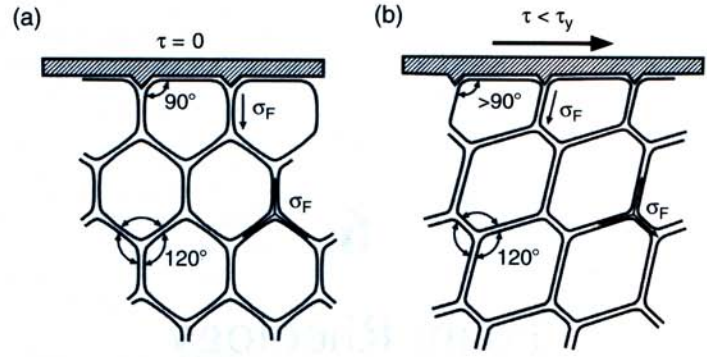

Fig. 6.1 *Schematic presentation of the origin of elastic response of foam, subject to shear stress, τ, lower than the foam yield stress, τ_y. (a) In the absence of external stress, the bubbles are symmetrical and the tensions of the foam films, σ_F, are balanced both inside the foam and at the confining solid wall. (b) At low external stress, the bubbles deform and the resulting slope of the foam films creates elastic shear stress inside the foam and in the contact zone foam–wall. Due to the preserved static angles between the foam films, 120°, the forces acting on each bubble are again balanced, despite bubble deformation.*

size, the foam tends to slip on the wall. In this case, the velocity of the first layer of bubbles in contact with the wall and the wall velocity do not match, in contrast to what is observed with simple liquids [4, 5, 14–20]. If this wall slip is not accounted for properly, it can lead to artefacts in rheological measurements aimed at determining bulk foam properties. Wall slip can also be useful, e.g. for foam transportation through pipes and for foam extrusion through orifices. The rheological properties of foams are complex not only because both the elastic and the viscous responses are nonlinear functions of the applied stress, but also because shear localization (coexistence of moving and non-moving regions) may occur under certain conditions [21–26].

Foam rheology is of practical as well as of fundamental interest, because of its observed similarities with the behaviour of other concentrated dispersions of soft 'particles', such as emulsion droplets, microgel beads, or lipid vesicles [4, 8, 27–29]. These similarities could be the result of generic physico-chemical mechanisms, which are currently under active investigation.

Significant progress has been made towards the physical understanding of the rheological properties of foams [4, 7, 8, 12, 14, 30, 31]. The elastic response is due to surface tension effects: each foam film bears a mechanical tension, σ_F, approximately equal to twice the surface tension of the liquid, σ, from which the foam is generated. If shear stress is applied externally, the bubbles are deformed, as illustrated in Fig. 6.1. As a consequence, the average orientation of the films is biased in the direction of the applied shear. This gives rise to an elastic stress inside the foam, which balances the applied stress (see Fig. 6.1(b)). As long as the external stress is smaller than the foam yield stress, τ_y, the films meeting at the Plateau borders are in static mechanical equilibrium and the bubbles are trapped in a self-supporting structure.

If the applied stress is strong enough to separate neighbouring bubbles, the foam structure yields, a steady shear flow sets in, and the bubbles slide along each other (see Fig. 6.2). The

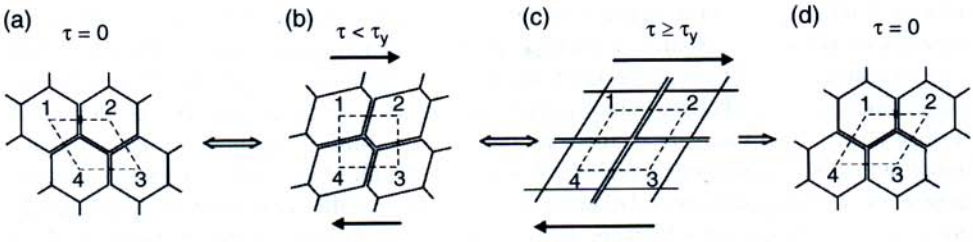

Fig. 6.2 *Schematic illustration of foam yielding and plastic deformation, under applied shear stress, which increases from (a) to (c) [4, 30]. The structure shown on image (c) illustrates the largest possible elastic deformation of the foam structure (presented here for 2D foam). This structure can relax either elastically, by returning to structure (a), or by a bubble rearrangement, leading to structure (d). This latter configuration is similar to structure (a), but the top bubble layer is shifted irreversibly with respect to the bottom layer, thus changing the bubble packing topology. Note the neighbour switching between bubbles 1 and 3, which became neighbours instead of 2 and 4. This topological change is called a 'T1 event' in dry foam. The viscous friction in the sheared foam films and Plateau borders between the moving neighbouring bubbles leads to energy dissipation and, hence, to viscous contribution to the shear stress.*

bubble rearrangements lead to local shear flow of the liquid inside the foam films and Plateau borders, resulting in dissipation of energy and a shear-rate-dependent (viscous) contribution to the macroscopic stress. If the applied stress is decreased back to zero, the flow stops and the bubbles relax towards a new equilibrium (see Fig. 6.2(d)). The macroscopic deformation, realized with respect to the initial stress-free structure, is called 'plastic strain'.

This review aims to present briefly our current understanding of the main phenomena involved in foam flow under steady and oscillatory shear deformation, and the main factors that control these phenomena. In addition, we track the links between the macroscopic rheological foam properties and the underlying processes at the microscopic scale. Only the simplest theoretical expressions are presented where available, to avoid mathematical complexity. The structure of the review is as follows: in Section 6.2 we outline the main experimental and theoretical approaches used to study foam rheology; in Sections 6.3–6.6 we discuss consecutively the foam visco-elasticity, yielding, plasticity, and steady viscous flow; in Section 6.7 we consider the foam-wall friction.

6.2 Main Experimental and Theoretical Approaches

Various experimental techniques are employed to characterize and analyse foam deformation and flow [4, 12, 14–16, 18, 32–34]. The macroscopic response to applied oscillatory or steady shear stress can be measured by rotational rheometers. Parallel plate, cone-plate and Couette cylinders have all been successfully used as shear geometries. However, several precautions must be taken to obtain physically interpretable rheological results. The surfaces of the confining walls must be roughened to avoid wall slip. Alternatively, one can use smooth surfaces and, in such cases, the foam-wall slip must be explicitly considered in

data analysis [31]. In addition, measures must be taken to ensure foam stability during the experiment, with respect to liquid drainage, bubble coarsening and liquid evaporation at the contact with ambient atmosphere. Only under such conditions are the gas volume fraction, mean bubble size, and bubble polydispersity well defined. These characteristics, along with surface tension and viscosity of the foaming solution (and sometimes the surface dilatational modulus; see Sections 6.6 and 6.7 below), must all be controlled to analyse quantitatively the rheological data and to compare the results for different systems. Alternatively, one can study the coupling between foam aging (due to bubble coarsening) and the rheological foam properties. In this case, the ageing process must be characterized for a foam sample, identical to that studied in the rheometer. For all these reasons, the rheological foam measurements are far from straightforward and the experimental protocols should be designed carefully, depending on the specific system and aim of the study.

Several complementary methods have been used to characterize the bubble velocity profiles and structural rearrangement dynamics in flowing foams. Magnetic resonance imaging (MRI) detects the velocity distribution inside sheared foam, while diffusing wave spectroscopy (DWS) provides statistical information about the rate of bubble rearrangements in strained and in flowing foams [18, 33, 35–38]. Direct optical observations of bubble monolayers (2D foams) have provided rich information about the bubble shape and dynamics in flowing foams [23, 24, 39–47]. Direct observations of dynamics inside dry 3D foams have been carried out using optical tomography [21]. Optical observations of isolated small bubble clusters have also provided valuable information about the bubble deformation and rearrangement in foams [48–50].

The experimental studies have clearly evidenced that the rheological response of foam involves processes in a wide range of length-scales. As already mentioned in Section 6.1, the deformation of individual bubbles creates the elastic stress of foams, while the yielding and plastic flow are the consequence of rearrangements in the bubble packing, and the viscous friction in the liquid films between neighbouring bubbles is a source of energy dissipation. At an even smaller structural scale, the stability and the mechanical response of the liquid–gas interfaces are governed by the adsorption of the foam stabilizers (surfactants, polymers, particles) [13, 16, 51–57]. At present, one of the most challenging and exciting research problems in foam rheology is to explain and predict the links between the macroscopically observed foam behaviour and the microscopic processes that govern this behaviour.

With this aim in view, the experimental results have stimulated the development of many theoretical models [4, 7, 11, 12, 17, 23, 24, 51, 52, 55, 58–68]. Two types of approaches are distinguished: continuum descriptions on a macroscopic scale, and physical models considering explicitly the foam microstructure. In the continuum models, the mechanical foam properties, such as elastic and viscous moduli, effective viscosity and yield stress, are incorporated phenomenologically in constitutive laws, which relate the stress, strain and rate of strain. Such constitutive laws are very useful to describe the macroscopic flow behaviour of foams, under various conditions. The physical models aim not only to construct constitutive laws, but also to predict foam rheological properties on the basis of the foam microstructure and local dynamics [23, 24, 46, 50–52, 63–66]. Additional insight has been gained by numerical simulations: the Surface Evolver software [69] has been used to determine foam equilibrium structures [70], as well as the stress in strained or flowing foams under quasistatic conditions [71, 72]. In this kind of numerical simulation, the interplay of rheology and coarsening can also be studied [73]. The viscous friction in foams is

currently simulated numerically by either the so-called 'bubble model' [63, 64] or the 'soft disk model' [61], which postulate linear dependence between the viscous stress and the relative velocity of the bubbles. For 2D foams confined by solid walls, the so-called 'viscous froth model' [74–76] is applied, which accounts explicitly for the viscous friction between the bubbles and the wall.

The following presentation briefly describes our current understanding of the main foam rheological properties, achieved by combining experimental and numerical work, as well as the theoretical approaches outlined above.

6.3 Foam Visco-elasticity

6.3.1 Linear Elasticity

Subjected to a sufficiently small shear strain, foam behaves like an elastic material and the stress τ varies linearly with the strain γ. In this linear regime, the bubbles are deformed, but the applied strain is too small to modify the topology of their packing. The specific surface area of the foam increases with the applied strain, and so does the volume density of bubble surface energy. The latter quantity scales as the tension of the gas–liquid interface, σ, divided by the average bubble size. Moreover, dimensional arguments show that the foam shear modulus, $G = \tau/\gamma$, scales as the surface energy density, multiplied by a prefactor, which depends on foam structure, polydispersity and liquid content [4]. The effects of these foam characteristics on the foam elastic modulus are considered below.

6.3.1.1 Monodisperse Dry Foam

We first consider ordered monodisperse dry foam, whose bubbles are assembled in a body-centred cubic structure (see Fig. 6.3). For this model system, called 'Kelvin foam' (see Chapter 3), the static shear modulus, averaged over all orientations of the sample,

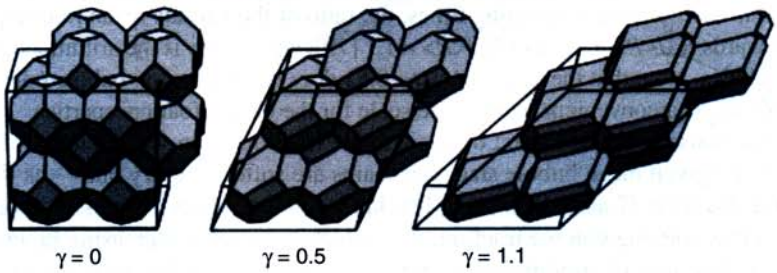

Fig. 6.3 *Dry Kelvin foam, subjected to a quasi-static shear strain γ, applied in the (100) direction. Each bubble has eight hexagonal films and six square films. Upon the deformation, the angles between the foam films, joining at a Plateau border, remain equal to 120°, and the angles between Plateau borders that join at a vertex are 109.5°, as required by Plateau's rules. The bubble deformation leads to an increase of the density of the surface energy in the foam (due to the increased bubble surface area) and to a resulting elastic response, characterized by the shear elastic modulus, G. Reproduced from [77], Editions Belin, Paris, 2010.*

has been determined in numerical simulations using the surface minimization code 'Surface Evolver' [69, 78]:

$$G = 0.51\frac{\sigma}{R} \tag{6.1}$$

$R = (3V/4\pi)^{1/3}$ is the radius of a bubble of volume V. For a typical foaming solution with $\sigma = 30\,\text{mN/m}$ and bubble radius $R = 100\,\mu\text{m}$, eqn (6.1) predicts a shear modulus $G = 150\,\text{Pa}$, illustrating that foams are soft materials.

Simulations of disordered monodisperse dry 3D foams yield a shear modulus close to that of a Kelvin foam. To analyse the physical origin of the prefactor in eqn (6.1), the structure of a disordered dry foam has been described as an ensemble of randomly oriented tetrahedral vertices, each connecting four Plateau borders. When these structures are sheared, their geometry evolves in agreement with Plateau's rules. A geometric calculation on this basis yields the relative change of interfacial area, as a function of the applied strain [65]. Using the specific surface area of random disordered monodisperse foams, $3.3/R$, obtained in numerical simulations [70], this model predicts a shear modulus $G = 0.55\sigma/R$, in good agreement with eqn (6.1) for ordered foam.

6.3.1.2 *Effects of Bubble Polydispersity and Liquid Content*

The volume to surface ratio of the bubbles sets a characteristic length scale in the foam (corresponding to the specific surface area of the bubbles) that governs foam elasticity. For polydisperse foam, this average ratio is conveniently represented by the so-called Sauter mean radius, $R_{32} = \langle R^3\rangle/\langle R^2\rangle$, which is determined by dividing the third moment of the bubble size distribution by its second moment. The Sauter radius is larger than the cubic mean bubble radius R_o, defined as $R_o = (3\langle V\rangle/4\pi)^{1/3} = \langle R^3\rangle^{1/3}$. The ratio R_{32}/R_o can be used as a quantitative measure of foam polydispersity. For a given mean bubble radius R_o, the elastic shear modulus decreases with increasing bubble polydispersity, as demonstrated in Fig. 6.4 by the simulation results for dry foams. In real foams, an increase of polydispersity with time arises, for instance, when an initially (almost) monodisperse foam ages by bubble coarsening. In this case, at long coarsening times, the ratio of the various mean radii typically converge towards $R_{32}/\langle R\rangle \approx 1.3$ and $R_o/\langle R\rangle \approx 1.1$ [79], where $\langle R\rangle$ is the arithmetic mean radius of the bubbles. Note that the ratio $GR_{32}/\sigma \approx 0.51$ does not depend on bubble polydispersity – therefore, R_{32} is a convenient bubble size scale for the elastic foam properties.

Let us discuss now the impact of gas volume fraction Φ on the elasticity of disordered foams. For a given mean bubble size, wet foams are softer than dry ones – as Φ decreases, the shear modulus G also decreases. The latter tends towards zero as Φ approaches the random close packing volume fraction, Φ_{CP}, which is a weakly increasing function of polydispersity. The loss of rigidity occurs when the packing reaches an isostatic mechanical equilibrium, where the bubbles are spherical and neighbours barely touch each other [80]. At $\Phi = \Phi_{CP}$, the foam can be sheared slowly without any interfacial energy 'cost'. Figure 6.5 shows experimental results for the dependence of the shear modulus of polydisperse foam on Φ, which are well described by the empirical relation [81]:

$$G = 1.4\Phi(\Phi - \Phi_{CP})\frac{\sigma}{R_{32}} \tag{6.2}$$

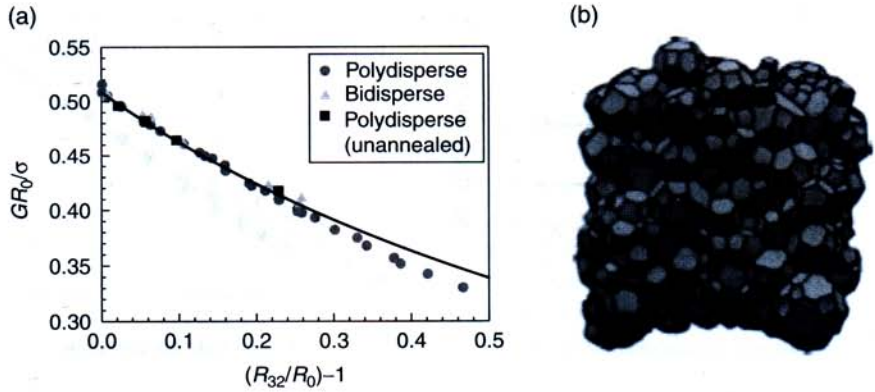

Fig. 6.4 *(a) Variation of the shear modulus G of disordered 3D dry foams, normalized by σ/R_o, with increasing foam polydispersity, characterized by the parameter ($R_{32}/R_o - 1$). The mean radius R_o is defined as $R_o = (3\langle V\rangle/4\pi)^{1/3}$ where V is the volume of a bubble in the foam. R_{32} is the mean volume-surface radius (Sauter radius). The continuous line is $GR_o/\sigma = 0.51R_o/R_{32}$. For monodisperse foam with $R_{32} = R_o = R$, the intercept with the ordinate axis corresponds to $G = 0.51\sigma/R$, in agreement with eqn (6.1). Data from [71]. (b) Structure of a dry polydisperse foam with $R_{32}/R_o = 1.15$, simulated using Surface Evolver software. Courtesy of A. Kraynik.*

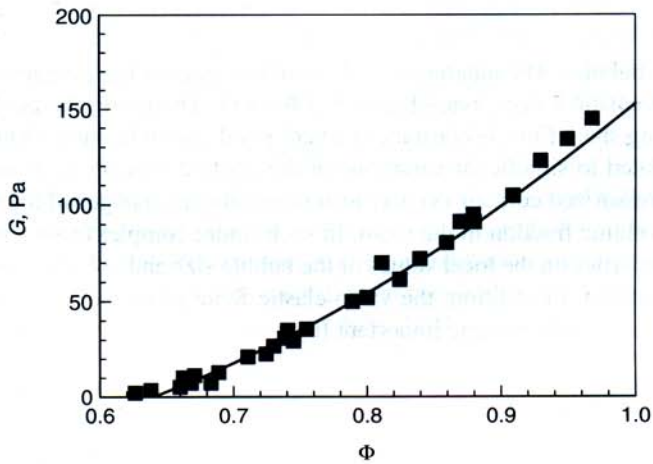

Fig. 6.5 *Shear modulus, G, versus gas volume fraction Φ, measured for 3D disordered polydisperse foams with $R_{32} = 66\,\mu m$, $\sigma = 20\,mN/m$, and $\Phi_{CP} \approx 0.64$. The continuous curve represents eqn (6.2). The Sauter mean radius R_{32} is determined from videomicroscopy measurements of the bubble diameter at the sample surface. Data from [81].*

with $\Phi_{CP} = 0.64$. For a dry foam ($\Phi = 1$), eqn (6.2) yields a numerical pre-factor of 0.50, similar to that predicted for monodisperse foam (cf. eqn (6.1)).

Foams are much harder to compress than to shear, and their Poisson ratio is very close to 0.5. Neglecting the water compressibility and the interfacial contribution, the foam compression modulus is given by the ratio K_T/Φ, where K_T is the compression modulus of the gas

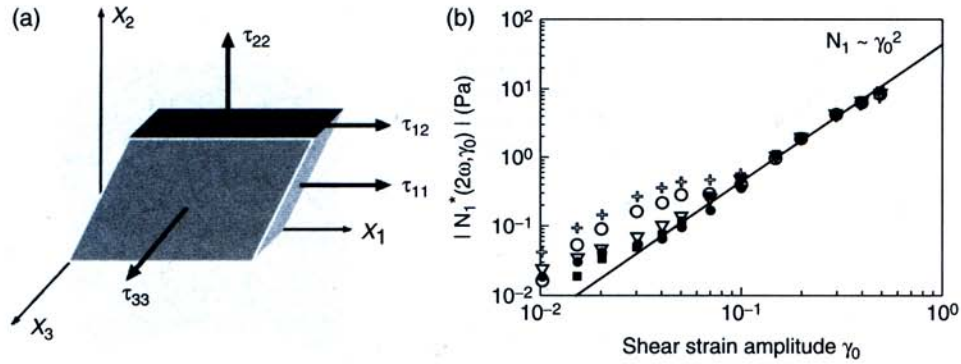

Fig. 6.6 *(a) A cube of foam is sheared in the X_1 direction. The arrows illustrate the components of the induced stress. (b) Amplitude of the first normal stress difference, N_1, induced by an applied oscillatory strain of amplitude γ_o, in a dry foam ($\Phi = 0.97$, average bubble radius $R = 80\,\mu m$, surface tension $\sigma = 27\,mN/m$, yield strain $\gamma_y = 0.4$). The foam is sheared in the gap of cone-plate geometry, with angle equal to 10° (open symbols) or 15° (filled symbols) at a frequency of 2 Hz. Note the quadratic dependence of N_1 on γ_o, except at low amplitudes, where deviations are seen due to residual trapped stresses. See more details in ref. [82], where these data are taken from.*

confined in the bubbles. The magnitude of K_T is of the order of the gas pressure outside the foam. Taking realistic values, one obtains $K_T/\Phi >> G$. Therefore, the bubble volume, in foam undergoing shear flow, is constant to a very good approximation. On the other hand, foam flows related to significant variations of the applied pressure (e.g. pumped flow or release from pressurized containers) may lead to significant changes of the bubble volume and of the air volume fraction in the foam. In such (more complex) cases, the dependence of the foam properties on the local values of the bubble size and volume fraction should be explicitly considered. In addition, the visco-elastic foam properties upon foam compression and expansion could become important [6].

6.3.2 Non-linear Elasticity

For larger strains, which are still too small to induce bubble rearrangements, foam film rotations and stretching lead to nonlinear mechanical response. For instance, shear deformation of a foam in the X_1 direction, as shown in Fig. 6.6(a), induces the shear stress component, τ_{12} (proportional to γ) and two normal stress differences, $N_1 = (\tau_{11} - \tau_{22})$ and $N_2 = (\tau_{22} - \tau_{33})$, which are observed to scale as γ^2. These differences arise because, with increasing strain, the foam films become predominantly oriented perpendicularly to the direction X_2. As a result, the surface tension of the foam films contributes more to the normal stresses τ_{11} and τ_{33}, and less to τ_{22}, thus leading to the normal stress differences N_1 and N_2 (see Fig. 6.6(a)).

A quantitative model of this effect, in quasistatically strained dry disordered 3D foams, was developed using the formalism of large deformation continuum mechanics. It predicts

a constitutive law of the Mooney–Rivlin form [66], in a good agreement with the results from the numerical simulations (cf. Fig. 6.12(a) below):

$$\tau_{12} = G\,\gamma \text{ (a)} \qquad N_1 = G\,\gamma^2 \text{ (b)} \qquad N_2 = -\frac{6}{7} G\,\gamma^2 \text{ (c)} \tag{6.3}$$

The results from oscillatory shear experiments, shown in Fig. 6.6(b), confirm that the amplitude of N_1 indeed scales with the square of strain amplitude, in agreement with eqn (6.3b). In addition, these data show that, at low strain amplitudes, internal stresses can remain trapped in the foam structure and modify the foam nonlinear response to strain – see the open symbols at strain amplitude $\gamma < 0.1$, which deviate from eqn (6.3b). These trapped stresses, which are enhanced with a small cone angle of the rheometer geometry, relax as the foam coarsens with time.

6.3.3 Linear Relaxations

Aqueous foams, subject to mechanical stress, not only store elastic energy – they can also dissipate energy, via viscous friction in the liquid contained in the foam films and Plateau borders, intrinsic viscous friction on the bubble surfaces and/or diffusive exchange of surfactant molecules between the solution and the air–water interface [55]. Here we focus on the regime where stresses and strains are so small that the viscoelastic response is linear and bubble rearrangements are not induced. For an applied oscillatory shear strain of amplitude γ_0 and angular frequency ω, $\gamma(t) = \gamma_0 \mathrm{Re}[e^{i\omega t}]$, the shear stress varies as $\tau(t) = \gamma_0 \mathrm{Re}[G^*(\omega)e^{i\omega t}]$, where $G^*(\omega) = G'(\omega) + iG''(\omega)$ is the complex shear modulus. The real part of the complex modulus accounts for the elastic foam response, whereas G'' accounts for the energy dissipation.

Figure 6.7 presents an example of the foam viscoelastic response over six decades in frequency. In the entire range of frequencies studied $G' > G''$, which reflects the predominant elastic behaviour of the foams. The data for G'' plotted in Fig. 6.7 show two relaxation processes, related to different mechanisms of energy dissipation. At low frequency (around 10^{-3} rad/s) a peak of G'' reveals a slow relaxation process with a characteristic time-scale of the order of $1/\omega \sim 10^3$ s. At high frequency (above 1 rad/s), there is a rapid increase of G'' with the frequency as $G'' \propto \omega^{1/2}$, in contrast to the expected behaviour for Newtonian viscous fluids, $G'' \propto \omega$. The physico-chemical origin of these two relaxation mechanisms is discussed below.

6.3.3.1 Slow Relaxation

Slow relaxations can be additionally probed by a creep experiment, where a stress step with amplitude $\tau_0 << \tau_y$ is applied to the sample, and the resulting strain $\gamma(t)$ is measured as a function of time. A typical creep response is illustrated in Fig. 6.8(a). After an instantaneous initial elastic response, steady flow sets in, even if the applied stress is very small. The strain evolution with time $\gamma(t) \cong \tau_o (1/G + t/\eta)$ is reminiscent of Maxwell fluid behaviour [84], with static shear modulus G and viscosity η. The ratio $t_0 = \eta/G$ gives the characteristic time of the slow relaxation process, which is of the order of several minutes for the data shown in Fig. 6.8. The peak of $G''(\omega)$ for such system is expected at a frequency $\omega_0 = 1/t_0 \approx 10^{-3}$ rad/s, in agreement with the results shown in Fig. 6.7.

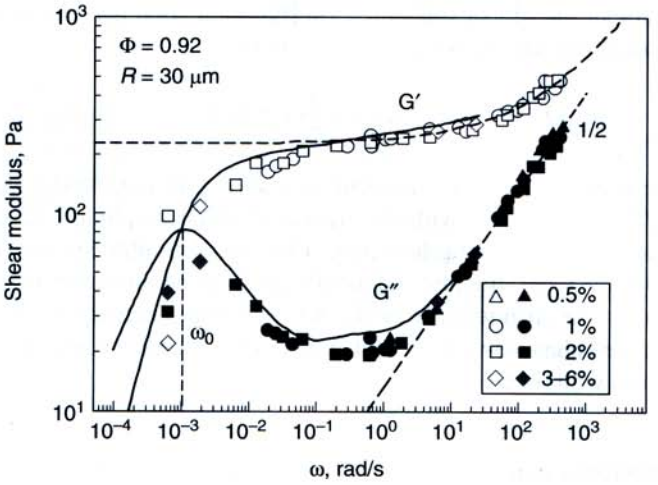

Fig. 6.7 *Dependence of the elastic G′and loss G″ shear moduli on oscillation frequency. The symbols correspond to different strain amplitudes as indicated in the legend. The dashed lines are a fit to* $G^*(\omega) = G(1 + (i\omega/\omega_c)^{1/2})$, *with* $G = 230\,Pa$ *and* $\omega_c = 156\,rad/s$. *The sample is Gillette shaving foam. Data from [83].*

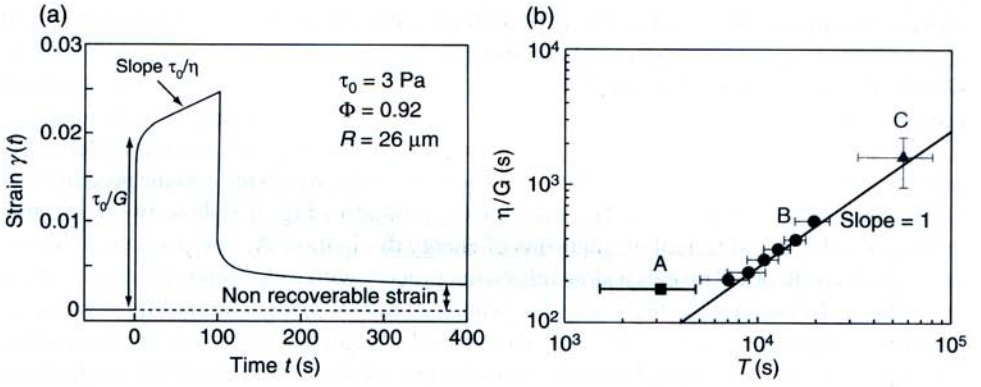

Fig. 6.8 *(a) Time evolution of the shear strain during a creep experiment with foam. A step stress,* τ_0, *is applied at* $t = 0\,s$, *during a time interval* $\Delta t = 100\,s$. *This stress is released at* $t = 100\,s$, *so that no stress is applied beyond this time.* Δt *is chosen short enough so that the average bubble size does not vary significantly during* Δt, *but long enough for numerous coarsening-induced bubble rearrangements to occur. The sample is Gillette (normal) shaving foam, sheared in a Couette cell with rough surfaces. Its steady creep behaviour is characterized by the parameters* $G = (150 \pm 10)\,Pa$ *and* $\eta = (66 \pm 6)\,10^3\,Pa\,s$.
(b) Characteristic time of the steady creep $t_o = \eta/G$, *as a function of the average time interval, T, between coarsening-induced rearrangements in a volume* $(2R)^3$, *for different foams with the same gas volume fraction,* $\Phi = 0.92$. *From A to C, the solubility of the gas in the foaming solution and, hence, the rate of coarsening-induced rearrangements decreases. The straight line is a linear fit:* $t_o = T(2R)^3/V_r$, *with the foam volume affected by a rearrangement being* $V_r = (6R)^3$, *i.e. about 50 bubbles. See details in [85].*

The low frequency response is related to the foam ageing, as the bubbles coarsen due to diffusive gas exchange between neighbouring bubbles (Ostwald ripening). This effect leads to intermittent local bubble rearrangements, which induce small random jumps of the macroscopic strain $\gamma(t)$ [83]. If shear stress is applied to the foam, the orientation of these jumps is biased towards the direction of the stress [73] and the foam flows steadily with a creep rate $\dot{\gamma}/\tau_o = 1/\eta$, given by the scaling law [72, 85]:

$$\frac{1}{\eta} \cong \alpha \frac{r V_r}{G} \tag{6.4}$$

Here r is the average number of coarsening-induced bubble rearrangements per unit time and unit volume, V_r is the typical foam volume affected by single rearrangement event, and α is constant of the order of unity. The time interval between coarsening-induced bubble rearrangements in a volume V_r is given by $T = 1/(rV_r)$. Using multiple light scattering, combined *in situ* with rheological creep measurements, eqn (6.4) has been validated [85]. Fig. 6.8(b) shows indeed good agreement between the data and eqn (6.4) with $V_r = (6.6\langle R\rangle)^3$. Therefore, eqn (6.4) links the slow rheological response of foams, expressed by the time $t_o = h/G = 1/\omega_o$, to their coarsening dynamics which sets the time T. As the foam coarsens, its rearrangement dynamics slows down and T increases with foam age t_w as $t_w^{0.66}$ [86, 87]. As a consequence, the relaxation frequency ω_o decreases as $t_w^{-0.66}$ [85]. Note that along the coarsening, the foam softens and its elastic modulus G decreases as described by eqn (6.2), due to the increase of the average bubble size.

6.3.3.2 Fast Relaxation

The anomalous non-Newtonian dissipation, observed at frequency higher than 1 rad/s in Fig. 6.7, is due to fast relaxations, coupled to the viscoelastic properties of the bubble surfaces that can promote either adhesion or sliding between adjacent bubbles [50]. In this range of frequencies, the complex foam modulus varies as:

$$G^*(\omega) = G\,(1 + (i\,\omega/\omega_c)^{1/2}) + i\,\eta_\infty\,\omega \tag{6.5}$$

in agreement with a theoretical model, based on randomly oriented weak zones in the foam [67]. In these weak zones, the bubbles slide with respect to each other when a macroscopic shear strain is applied, instead of undergoing affine deformation. This collective relaxation process exhibits a characteristic relaxation frequency, ω_c, set by the interplay between an elastic storage modulus and a viscous dissipation, and depending on the interface 'rigidity' [55] (the latter can be characterized by the surface dilatational modulus of the foaming solution, see section 6.6 below and Refs. [16, 54]). The Newtonian viscosity η_∞ (eqn 6.5) is expected to dominate G^* at very high frequencies, and should scale with the viscosity of the foaming solution η_0.

As illustrated in Fig. 6.9, experiments with a series of different foaming solutions show that ω_c exhibits different scaling laws with shear modulus G, or equivalently with the bubble size R, depending on the rigidity of the liquid–gas interfaces. Theoretical modelling of these processes predicts that the energy dissipation is dominated by Marangoni flow in the foam films between the bubbles for foams with 'rigid interfaces' (i.e. those having high surface dilatational elastic modulus), whereas for mobile interfaces (low surface modulus) the dissipation

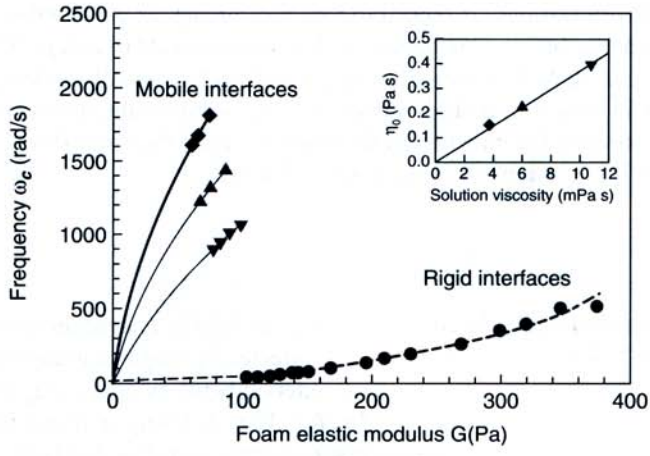

Fig. 6.9 *Characteristic frequency ω_c of the fast collective relaxation process versus shear modulus G, for foams with (●) rigid interfaces (Gillette shaving foam) and with mobile interfaces (SLES/CAPB) containing Glycerol of (◆) 40wt%, (▲) 50wt%, and (▼) 60wt%. The gas volume fraction is the same for all of these foams: $\Phi = 93\%$. We recall that $G \propto \sigma/R$ according to eqn (6.1). The dashed line represents the scaling law, $\omega_c \propto Eh/\eta_0 R^2$, whereas the continuous lines correspond to the law, $\omega_c \propto \sigma/(\eta_0 R + \kappa)$, with E and κ being the dilatational surface elasticity and viscosity respectively, and h being the film thickness. See details in [56]. The insert shows the solution viscosity deduced from the fits of the SLES/CAPB data to the scaling law (b), compared to the viscosity measured independently. The error bars are comparable to the size of the symbols.*

is dominated by marginal flow of liquid withdrawn from or receding into the Plateau borders [56]. The model predicts also that the foam loss modulus is independent of the bubble size in the case of rigid surfaces, $G''_{rigid} \propto (\eta_0/Eh)^{1/2}$, where E is the dilatational surface modulus and h is the foam film thickness. In contrast, the foam loss modulus decreases with R for mobile surfaces as $G''_{mobile} \propto (\eta_0/\sigma R)^{1/2}$ (after neglecting the contribution of interfacial viscosity).

Therefore, to formulate foam with maximal dissipation of mechanical energy upon oscillatory shear, one should increase the solution viscosity and the interfacial rigidity, since we generally have $Eh << \sigma R$ for a given bubble size and gas volume fraction. This prediction may be of practical relevance for foams used as mechanical attenuators.

6.3.4 Shear Modulus of Particle-laden Foams

The experiments with particle-laden foams [88] showed that solid particles, comparable in size to the foam bubbles, enhance strongly the linear foam elasticity – much more than homogenization arguments in the framework of continuum mechanics would predict. This is due to the capillary interactions between the particles captured within the foam structure [88]. In contrast, the yield stress of the foam does not exhibit such an anomalously large enhancement. The rheology of foams, stabilized by particles that are much smaller than the bubble size, has not been investigated systematically so far, but it may be expected to be similar to that of particle stabilized emulsions [89].

6.4 Yielding

When foams are subjected to increasing shear stress or strain, they exhibit a transition from solid-like to fluid-like behaviour, called 'yielding' [90]. Figure 6.10(a) shows a typical stress response to steadily increasing applied shear strain. As described in the previous section, the stress first increases, as in an elastic solid. Afterwards, the stress passes through weak maximum and finally settles at a plateau. In this latter regime, the stress (the height of the plateau) is an increasing function of the applied shear rate, $\dot{\gamma}$. The stress threshold, beyond which the flow sets in, is called 'yield stress' and is denoted by τ_y. The corresponding strain threshold is the yield strain, denoted by γ_y (see Fig. 6.10(a)).

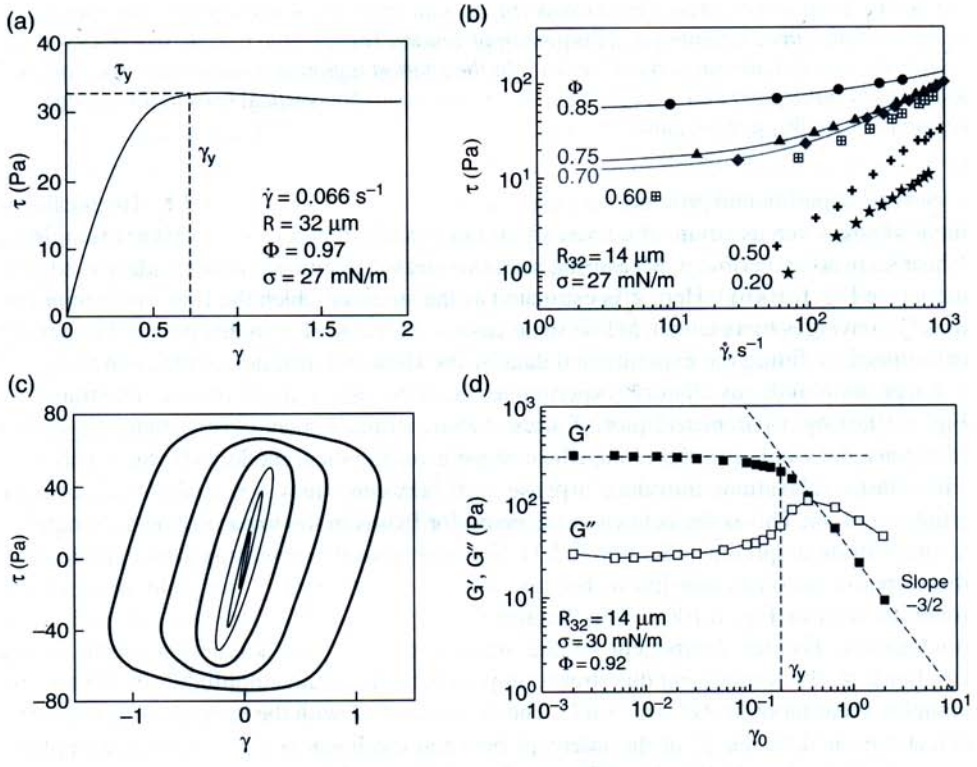

Fig. 6.10 *(a) Shear stress, induced by an applied shear strain, γ, that increases with time at constant rate [94]. (b) Shear stress, as a function of the strain rate, for several gas volume fractions. The data for Φ > 0.64 exhibit a plateau at low shear rates, indicating yield stress behaviour. The continuous lines are fits to the data using the Herschel–Bulkley law, eqn (6.7) [95]. (c) Shear stress versus strain, measured in an oscillatory experiment, at a frequency of 1 Hz [93]. The six curves correspond to increasing strain amplitudes of 0.055, 0.15, 0.25, 0.43, 0.72 and 1.2, respectively, and are drawn using lines of increasing thickness. The sample is the same as in (d), where its properties are specified. (d) Oscillatory response, represented as the dependency of the storage and loss moduli, G′ and G″, with the oscillation amplitude, γ_0. The angular frequency is ω = 2 rad/s. For $\gamma_0 > 0.5$, localized flow was observed in this experiment.*

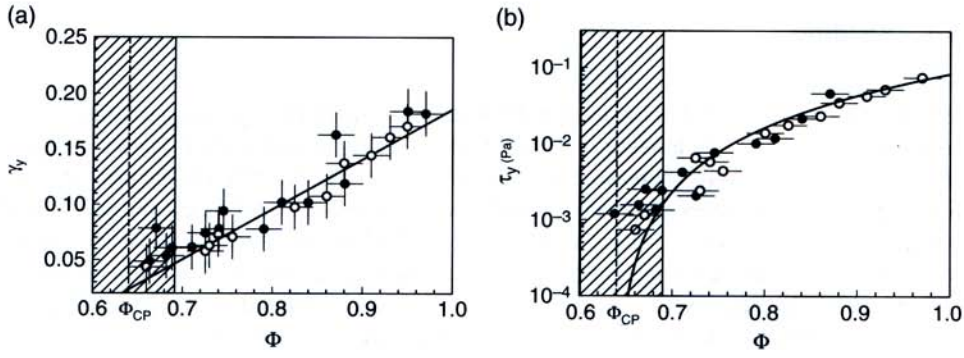

Fig. 6.11 *Yield strain (a) and yield stress (b), as a function of the volume fraction, measured in an oscillatory measurement at a frequency of 1 rad/s. The average bubble size is <R> = 55 μm, the surface tension is σ = 17 mN/m. In the shaded region, the water drainage from the foam could not be avoided, making these data unreliable. The vertical lines in the shaded region indicate $\Phi_{CP} = 0.64$. Data from [81].*

Several experimental protocols are used in practice to determine γ_y and τ_y. The measurement of stress versus strain, at a fixed strain rate (as illustrated in Fig. 6.10(a)) is called a 'shear start-up' experiment. Measuring stress versus strain rate is another widely used protocol (see Fig. 6.10(b)). Here τ_y is estimated as the stress at which the flow curve approximately converges to a plateau, at low shear rates – the value of τ_y in this protocol is usually determined by fitting the experimental data by the Herschel–Bulkley model, eqn (6.7).

Large amplitude oscillatory experiments (LAOS) are a third option, illustrated in Fig. 6.10(c) by a parametric plot of stress versus strain. For an elastic material, such a Lissajous plot yields a straight line, whose slope gives the shear modulus G (Section 6.3.1). Viscoelastic relaxations introduce a phase shift between stress and strain, leading to an elliptic contour. This is the behaviour observed for foams in the linear viscoelastic regime, at small strain amplitudes (Section 6.3.3). For progressively increasing strain amplitudes, the response becomes non-linear, because the stress is bound by the yield stress of the foam, as seen in Fig. 6.10(c). This feature is analysed quantitatively by calculating the fundamental Fourier component of the stress oscillation, as a function of the strain amplitude γ_0. By normalizing this stress component by the strain amplitude, one obtains the complex shear modulus $G^* = G' + iG''$. The decrease of G' with the increase of γ_o is used to detect the yield strain, γ_y, at the intercept between the linear regime and the asymptotic power law $G' \propto \gamma_0^{-3/2}$ [81, 91, 92] (see Fig. 6.10(d)). The yield stress is deduced as $\tau_y = |G^*(\gamma_y)|\gamma_y$. Since the variations of G^* with strain amplitude describe only the fundamental component of the stress response, they capture only partially the complete stress–strain relation shown in Fig. 6.10(c). Thus to be conclusive, a test of any non-linear rheological model requires a measurement of the full Fourier spectrum of the stress [93].

The dependence of the yield strain and yield stress on liquid volume fraction is illustrated in Fig. 6.11. Dimensional arguments suggest that the yield stress should scale with the bubble capillary pressure, σ/R, in agreement with the experimental results. Such scaling can be used also to compare the yielding properties of foams and emulsions, which turn out to be similar [4, 14, 92]. Technically, experiments with foams are rather difficult at $\Phi < 0.8$,

due to the water drainage from the foam, which destabilizes the samples. Experiments with emulsions, which are less prompt to drainage in this range of volume fractions, showed that the yield stress and strain both tend to zero as Φ approaches $\Phi_{CP} \approx 0.64$ [92]. For $\Phi < \Phi_{CP}$, the number of contacts between neighbouring bubbles (or drops) becomes too small to sustain static mechanical equilibrium, and an arbitrarily small stress induces steady flow. The dependence of the yield stress on bubble size, surface tension and dispersed volume fraction in foams and emulsions is described well by the following empirical law [81, 92]:

$$\tau_y = \beta \frac{\sigma}{< R >} (\Phi - \Phi_{CP})^2 \tag{6.6}$$

where β is a dimensionless coefficient close to 0.50 [12].

As illustrated schematically in Fig. 6.2 for a 2D foam, the foam yielding occurs at the scale of the individual bubbles when the applied macroscopic stress or strain is large enough to induce rearrangements in the bubble packing. For real polydisperse 3D foams, the bubble structure is more complex, but similar irreversible bubble rearrangements (called 'T1 events' for dry foam) lead to yielding and plastic flow of the foam.

So far, we have discussed the transition from solid-like to liquid-like behaviour only as a function of gas volume fraction and applied stress or strain. However, the experimental time scale, over which the mechanical response is probed, is another control parameter of the foam response. This time scale is set by the inverse frequency of an applied oscillatory strain or by the inverse strain rate for a steady flow. For sufficiently long time scales, so that the bubble coarsening induces a significant number of bubble rearrangements, foam flows like a highly viscous liquid even at very low stress, $\tau < \tau_y$ (cf. Section 6.3.3). Even if the experimental time scale is so short that coarsening is negligible, the time scale can still affect the yielding behaviour – shear start-up experiments showed that the critical strain and stress, at which the shear-induced bubble rearrangements are triggered, are increasing functions of the applied strain rate [21]. This dependence is related to the duration of the individual rearrangement events, which in turn is affected strongly by the visco-elastic properties of the gas–liquid interfaces [39, 48].

6.5 Plastic Flow

Plastic strain is defined as the irreversible deformation that occurs when a material is sheared beyond its yield strain. For a very slow plastic shear flow, one may expect the sample to relax almost instantaneously towards static equilibrium whenever the applied shear rate is released suddenly. Such behaviour is called 'quasi-static'. In practice, even very slow foam flows are quasi-static only approximately, due to the slow viscoelastic relaxations discussed in Section 6.3.

As an illustration of the plastic properties of a foam, Fig. 6.12 shows the evolution of several components of the stress tensor, as a function of the applied shear strain, obtained in a 3D numerical simulation of dry foam [71]. The stress–strain relationship is similar to the experimental results shown in Fig. 6.10(a), except for the abrupt small jumps, which are due to rearrangement events of the individual bubbles. These jumps cannot be resolved in

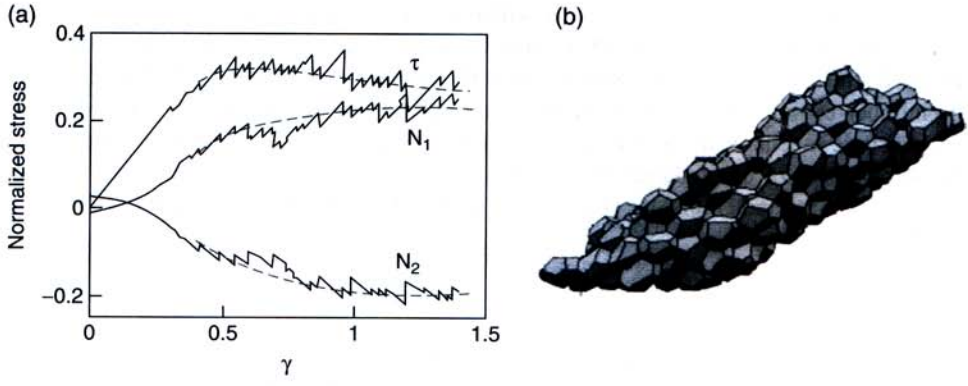

Fig. 6.12 *(a) Shear stress and normal stress differences versus shear strain, obtained in a quasi-static simulation using the Surface Evolver software. The sample is 3D disordered monodisperse dry foam containing 216 bubbles. The dashed curves, drawn at $\gamma > 0.4$, are guides to the eye. The quantities τ, N_1 and N_2 are normalized by $\sigma/V^{1/3}$ where V is the volume of a bubble. (b) Structure of the sheared foam. Data from [64].*

the experimental measurements with a macroscopic foam sample, because the latter contains a much larger number of bubbles than those used in the numerical simulation. Figure 6.12 shows also that the normal stress differences are similar in magnitude to the shear stress in the steady flow regime. This is in agreement with the theoretical predictions [82]. Normal stress differences arise in many flowing visco-elastic materials, and they are of practical importance in extrusion flows, for instance [84]. However, in contrast to many polymeric liquids, the normal stress differences N_1 and N_2 in flowing foams are of similar magnitude and opposite signs.

As a first step towards a general constitutive law, relating stress and strain in rearrangement-driven plastic flow, the elementary plastic events have been modelled as force dipoles acting on an elastic continuum [68], in a good agreement with numerical simulations [42]. In another approach, so far limited to 2D foams, the anisotropy of the foam microstructure is captured by a texture tensor related to the macroscopic stress [45]. The striking similarity between the rheology of glasses and many complex fluids, including foams, has stimulated the development of another general model (called the 'soft glassy rheology' model), which captures the non-linear elastic and plastic response of yielding foams [93]. In addition, several phenomenological models have been proposed, which extend the elasto-plastic constitutive laws by including relaxation terms describing the visco-elastic foam behaviour [96].

6.6 Viscous Dissipation in Steadily Sheared Foams

The stress in steadily sheared foam depends on the applied shear rate. Experiments have shown [4, 16, 18, 31, 52] that this behaviour is usually represented well by the Herschel–Bulkley equation (see Fig. 6.13a):

$$\tau(\dot{\gamma}) = \tau_y + \tau_v(\dot{\gamma}) = \tau_y + k\dot{\gamma}^n \tag{6.7}$$

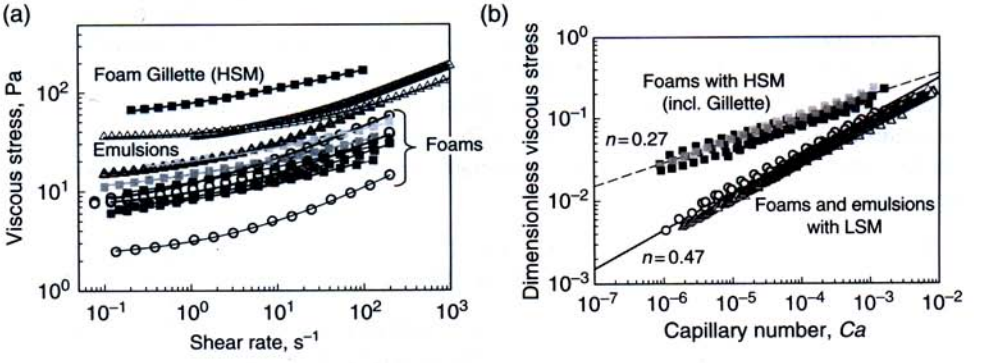

Fig. 6.13 *(a) Experimental results for the dependence of shear stress, τ, on shear rate, $\dot{\gamma}$, for steadily sheared foams and emulsions. The open circles denote foams with low surface modulus, the filled squares foams with high surface modulus and the open triangles emulsions with low surface modulus. For the foams, the bubble radius varies between 20 and 300 μm, surface tension varies between 22 and 30 mN/m, and viscosity of the continuous phase is varied between 1 and 11 mPa.s by adding glycerol in the aqueous phase. For the emulsions, the drop radius varies between 2 and 40 μm, interfacial tension varies between 2 and 10 mN/m, and viscosity of the drop phase varies between 2 and 5 mPa.s. For all systems, the bubble (drop) volume fraction is 0.90 ± 0.01. The curves are fits by the Herschel–Bulkley model, eqn (6.7). (b) Dimensionless viscous stress, $\tilde{\tau}_V$, v. capillary number, Ca, for the same systems. Two different types of flow behaviour are evidenced, characterized by different values of the power-law index,* n.

which contains three characteristic parameters: the yield stress τ_y, the power-law index n and the consistency k. Here, $\tau_V(\dot{\gamma})$ is the rate-dependent part of the total stress, determined by subtracting τ_y from the total stress, $\tau(\dot{\gamma})$. For foams and concentrated emulsions with $\Phi > \Phi_{CP}$, the power-law index, n, is typically between 0.2 and 0.5, reflecting the strong shear-thinning behaviour of these systems [16, 18, 31, 52]. The dimension of the consistency k is Pa.s^n and it is, therefore, dependent on the specific value of n. The flow behaviour of Herschel–Bulkley fluids in different geometries (through pipes, between Couette cylinders, etc.) is described in rheology textbooks [84, 97] and will not be recalled here.

When comparing experimental results for various systems and with theoretical predictions, it is convenient to use appropriate dimensionless quantities. The viscous stress is scaled by the mean capillary pressure of the bubbles, $\tilde{\tau}_V = \tau_V R_{32}/\sigma$. The shear rate is scaled by the ratio of the viscous stress and bubble capillary pressure, leading to the so-called 'capillary number', $Ca = (\eta\dot{\gamma}R_{32})/\sigma$. This number plays the role of a dimensionless shear rate in this context. Comparing shear flow data for different systems, plotted in terms of the dimensionless quantities $\tilde{\tau}_V$ and Ca, eliminates the generic effects of R_{32}, σ, and η. Such a representation highlights the specific influence of the type of dispersion (foam or emulsion), surfactant type [14–16] or other specific features, if present.

As an example, we show in Fig. 6.13(b) experimental data $\tilde{\tau}_V(Ca)$, for a variety of foams and concentrated emulsions with different values of R_{32}, σ and η. The requirements met by all the experimental data compiled on this graph are: (i) the continuous phase of the foam or the emulsion is Newtonian; (ii) wall slip was suppressed so that the true foam flow curve

was measured; (iii) data about the mean bubble or droplet size, interfacial tension and solution viscosity are available, so that the final results can be presented in dimensionless form; (iv) the mean radius of the drops and bubbles is larger than about 2 μm to avoid possible effects of surface forces acting in the foam and emulsion films (see [52] for numerical estimates about the effect of surface forces). Remarkably, all these data collapse onto two master curves, when plotted in this dimensionless representation. Thus we can distinguish two qualitatively different cases:

1. Systems in which the power-law index is $n \approx 0.45 \pm 0.03$ [16, 18, 31, 33, 51, 52, 54, 98].
2. Systems where n is close to 0.25 ± 0.05 [16, 18, 51, 52, 54, 99].

For similar characteristics Φ, η, σ and R_{32}, type 2 systems exhibit much higher viscous friction compared to those of type 1 [14, 16, 52]. Moreover, local velocity measurements using MRI techniques showed that the foams of both types exhibit flow that is described well by the Herschel–Bulkley law (eqn 6.7), without observable indications of shear banding [35] for gas volume fractions in the range 0.88–0.95. Similar findings were reported for emulsions [33].

Experiments comparing the interfacial properties of the foaming solutions [16, 52] showed that the principal difference between systems of type 1 and 2 is the magnitude of their surface dilatational modulus, E. This parameter characterizes the amplitude of surface tension variation, induced by a sinusoidal perturbation of the solution surface area. For all systems of the first type (with $n \approx 1/2$) the surface modulus, measured at frequencies of the order of 0.1 Hz, is low, $E < 10$ mN/m [16, 52]. In contrast, the surface modulus is much higher for the systems of the second type, $E > 100$ mN/m [16, 18, 52]. These results show that the predominant mechanisms of viscous dissipation in foams, stabilized by surfactants with low surface modulus (LSM) and by surfactants with high surface modulus (HSM), are different. Therefore, to compare and discuss experimental data obtained with different foaming solutions, the solution surface properties (including its surface modulus) must be characterized and taken into account. It is worth noting that some commercial foams used widely in rheological studies (e.g. Gillette shaving foam) are formulated to have HSM, whereas other foaming systems (e.g. dishwashing liquids) usually have LSM.

Theoretical modelling showed that the experimental data could be described by considering two principal mechanisms of viscous dissipation of energy in sheared foams: (i) in the foam films, formed between two neighbouring bubbles, and (ii) in the surfactant adsorption layers on the bubble surfaces [51, 52]. These two mechanisms are considered consecutively below.

6.6.1 Predominant Viscous Friction in the Foam Films

Let us consider first the viscous dissipation of energy in the foam films, which is due to the relative motion of the bubbles with respect to each other, and which is the prevailing mechanism of energy dissipation for foams stabilized by LSM surfactants. The relative bubble motion creates local velocity gradients in the fluid confined in the foam films; see Fig. 6.14. The theoretical modelling showed [52] that the liquid motion inside the sheared foam films could be decomposed into two coexisting 'elementary' processes:

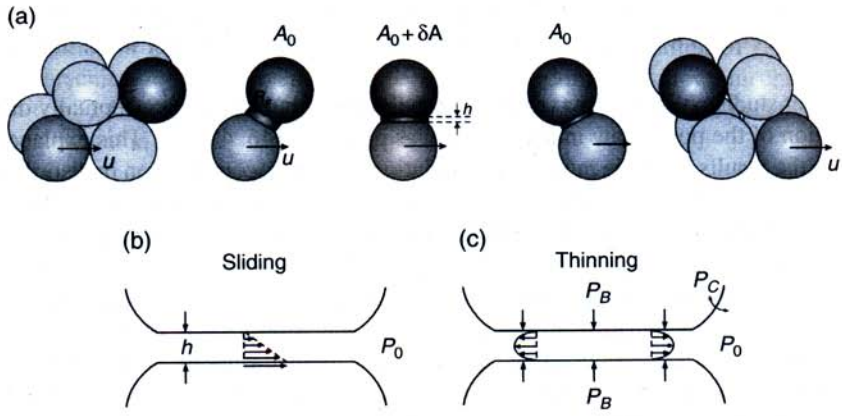

Fig. 6.14 *(a) Schematic presentation of the processes of formation, thinning, and disappearance of a foam film between two bubbles in sheared foam [51, 52]. Note that the process of formation and expansion, and the subsequent shrinking and disappearance of the foam film, is accompanied by a change in the total surface area of the colliding bubbles. (b) Schematic presentation of the process of sliding: opposite film surfaces move at different velocities, driven by the relative motion of neighbouring bubbles in flowing foam. The film thickness* h *determines the local shear rate of the liquid in the film. (c) Schematic presentation of film thinning. This process is driven by the excess of pressure in the bubbles,* P_B*, as compared to the pressure in the liquid outside the film,* P_0*. The viscous dissipation is predominantly due to the sliding motion.*

(i) sliding motion of the opposite film surfaces, driven by the relative motion of the neighbouring bubbles in sheared foam (Fig. 6.14(b)); (ii) thinning of the foam film, which is due to the higher dynamic pressure inside the film (imposed by the capillary pressure of the bubbles, P_C), as compared to the pressure in the surrounding Plateau channels; see Fig. 6.14(c).

The numerical estimates showed that the main dissipation of energy in the foam films is due to the sliding motion of the bubbles, i.e. to process (i) [52]. However, the film thinning process (ii) should be also considered explicitly, because it determines the instantaneous film thickness and the resulting velocity gradient inside the foam film. Using a standard hydrodynamic approach and reasonable assumptions, the rate of energy dissipation inside the foam films was calculated and used to derive an approximate formula for the viscous stress in sheared foams [51, 52],

$$\tilde{\tau}_{VF} \approx 1.16 Ca^{0.47} \Phi^{5/6} (\Phi - 0.74)^{0.1} / (1-\Phi)^{0.5} \tag{6.8}$$

$\tilde{\tau}_{VF} = \tau_{VF} R_0/\sigma$ is the dimensionless shear stress, related to the friction in the foam films (the subscript *VF* denotes viscous friction inside the films). This model predicts $n \approx 0.47$, which is in a very good agreement with the experimental results for LSM systems. Despite the fact that the theoretical model assumes ordered and monodisperse foam structure, it was verified experimentally that eqn (6.8) is applicable to both disordered monodisperse and polydisperse foams and emulsions, if the assumptions used to derive eqn (6.8) are satisfied (e.g. the surface forces between the foam film surfaces are negligible [52]). These

experimental tests were carried out in the range of volume fractions $0.8 < \Phi < 0.98$. In addition, for eqn (6.8) to be valid, the shear rate must be sufficiently high, as discussed below.

In recent studies of 2D foams (sheared monolayers of bubbles), a conceptually different explanation of the power-law index $n \approx 1/2$ was proposed [46, 47, 61]. This explanation is based on the results from the numerical simulations of the viscous friction in disordered 2D foams using the 'bubble model' [63, 64]. This model assumes that the friction force between neighbouring bubbles depends linearly on their relative velocity, and that the friction coefficient is independent of the shear rate [62] (in contrast to the model leading to eqn (6.8)). For the macroscopic stress induced by steady shear of the foam, a power-law index $n=0.54$ was obtained from the numerical simulations, made under these assumptions. Thus, friction forces depending linearly on the relative velocity of neighbouring bubbles can give rise to macroscopic non-Newtonian viscous behaviour. The simulations showed also that the bubble trajectories are highly irregular in the investigated range of low shear rates. The link between local and macroscopic viscous dissipation in 2D foams was also investigated experimentally, using bubble rafts floating on a liquid surface [46, 100]. The local viscous interaction between neighbouring bubbles was in this case found to be a non-linear function of the relative bubble velocity, with a power-law index that was again different from the one deduced from the macroscopic foam flow data. Both the experimental and the simulation work led to the suggestion that the disorder of the foam structure may have a strong impact on foam rheology, and that the highly irregular bubble motion observed in flowing 2D foams can be the origin of the observed difference between the macroscopic and the local friction laws.

These findings raise the question whether irregular bubble motion in disordered 3D foams may also have a strong impact on the non-linear macroscopic viscous dissipation, or whether the mechanism leading to eqn (6.8), which does not take into account the bubble disorder, is dominant. As evidenced by the experimental results and theoretical analysis, the answer may depend on the foam shear rate: light scattering experiments with sheared 3D Gillette foam showed that the bubble dynamics was intermittent at rates below $0.5\,s^{-1}$, suggesting irregular motion reminiscent of the one discussed above for 2D foams. In contrast, the flow was found to be approximately laminar at higher shear rates [37], in qualitative agreement with the observations of bubble trajectories at the surface of rapidly sheared foams, as reported in [14]. As discussed in ref. [14] (see eqn (6.14) and the related discussion therein) this transitional shear rate might be explained by comparing the characteristic time for film thinning with the contact time of the bubbles (the latter is approximately equal to the inverse shear rate of the foam) – in slowly sheared foams, the foam films have enough time to thin down to their equilibrium thickness, h_{EQ}. In contrast, the bubbles are in contact very shortly in rapidly sheared foams, so that the transient foam films formed between colliding bubbles have no time to thin down to h_{EQ}. In this regime, the theoretical model predicts [52] that the thickness of the transient foam film scales with $Ca^{1/2}$, i.e. it significantly increases with the shear rate. Depending on the system parameters, the threshold shear rate, separating these two different regimes of foam flow, is expected to be of the order of 0.01 to $1\,s^{-1}$ [14]. These results suggest that the assumptions used to derive eqn (6.8) are best verified at high shear rates. Indeed, most of the published flow curves for 3D foams were measured at high shear rates, whereas 2D foams have been studied mostly at low shear rates. Data where the viscous contribution to the shear stress

in 3D or 2D foam is resolved well enough to establish accurately the power law exponents in *both* regimes would clearly be of interest. We recall that in the limit of very low shear rates, coarsening-induced creep flow becomes the dominant flow mechanism (see Section 6.3.3). In this regime, the flow index is equal to 1 and the foam flows like a very viscous Newtonian fluid.

6.6.2 Predominant Viscous Friction in the Surfactant Adsorption Layer

The viscous stress, measured under the same conditions for foams stabilized by HSM surfactants, is much higher than in foams stabilized by LSM surfactants. This result shows that an additional contribution into the viscous stress must exist for these systems. Theoretical arguments show that the bubble collisions in sheared foams lead to oscillations of the bubble surface areas around their mean value, A_0. This variation of the bubble surface area leads to viscous dissipation of energy in the surfactant adsorption layer, due to the surface dilatational viscosity. The following expression was derived theoretically for this contribution (denoted as τ_{VS}) to the total viscous stress [52]:

$$\tilde{\tau}_{VS} \equiv \tau_{VS} R_0 / \sigma \approx 9.8\Phi(E_{LD} / \sigma)\Phi a_0^2 \tag{6.9}$$

E_{LD} is the surface dilatational loss modulus of the adsorption layer (viscous surface modulus) and a_0 is the relative amplitude of the bubble area oscillations. In general, the viscous stress in sheared foams includes contributions from the energy dissipation in both the foam films and adsorption layers: $\tau_V = \tau_{VF} + \tau_{VS}$. However, the second contribution is important for HSM systems only [52].

Two series of experimental results, obtained with different types of foam samples, deserve additional discussion.

Soller and Koehler [32] studied the rheological properties of draining foams, maintained in a stationary state by continuous perfusion of surfactant solution at the top of the foam. The measured flow curves were incompatible with the Herschel–Bulkley model, in contrast to other results obtained under conditions where drainage is insignificant. The most probable reason for this difference is that the film thickness is modified in the presence of liquid drainage in the foam, as previously reported [101]. Since the friction between neighbouring bubbles depends on film thickness, liquid drainage is indeed expected to affect the bubble–bubble friction and the resulting foam viscous stress. The results obtained in [32], concerning the specific rheological properties of draining foams, could be of specific interest in several practical applications.

Pilon and co-workers studied foam rheology at lower volume fractions experimentally (Φ varied between 0.54 and 0.70) [102, 103]. The foam viscous stress was determined by pipe-flow rheometry and the power-law index n was found to be in the range between 0.60 and 0.66 for all foams studied. The authors interpreted these data as a dependence $\tau_V \propto \mathrm{Ca}^{2/3}$ (i.e. $n \approx 2/3$), which was assumed to be a result of predominant friction in curved meniscus regions [103]. Firmly established theoretical models for foam viscosity at low volume fractions are not yet available. Moreover, the authors' claim that there was no wall slip in their experiments deserves more convincing verification. An interesting observation in this study was that the viscous friction depended strongly on bubble polydispersity,

most probably, because Φ was around the value of Φ_{CP}. In contrast, the experimental results obtained by other authors at $\Phi \geq 0.80$ did not indicate a strong dependence of the viscous stress on bubble or drop polydispersity [16, 31, 52].

6.7 Foam–Wall Viscous Friction

If foam is in contact with a smooth solid wall, the application of external stress often leads to sliding of the boundary bubbles along the wall surface, thus violating the common 'non-slip' boundary condition for fluid flow at solid surfaces, see Fig. 6.15 [4, 7–9, 15–18]. This 'foam-wall slip' phenomenon may affect strongly the rheological measurements because, in its presence, the actual shear rate inside the foam cannot be deduced directly from the motion of the walls bounding the sample.

Foam-wall slip is conveniently studied by placing the foam in contact with a smooth solid surface in the rheometer (e.g. with the wall of a Couette cylinder, plate, or cone) and applying an external stress that is lower than the yield stress of the foam [15–18]. Under these conditions, foam-wall slip with controlled slip velocity is obtained, and the measured shear stress is entirely due to the viscous friction of the boundary layer of bubbles with the wall surface. A similar type of viscous friction is observed when bubbles or drops travel along a narrow capillary tube (so-called 'Bretherton problem'). The latter configuration is relevant to several important applications, such as enhanced oil recovery by surfactant solutions and microfluidics [5, 7, 9, 19, 106–110].

The measured foam-wall stress, τ_w, is conveniently scaled by the bubble capillary pressure, $\tilde{\tau}_w = \tau_w R_{32}/\sigma$, while the relative foam-wall velocity, V_0, is represented in dimensionless form by the wall capillary number, $Ca^* = \eta V_0/\sigma$. The experimental results for $\tilde{\tau}_w$ v. Ca^* are well represented by a power law, $\tilde{\tau}_w = k_w(Ca^*)^m$; see Fig. 6.16. These experimental results also provide evidence that the foam-wall yield stress is usually negligible in

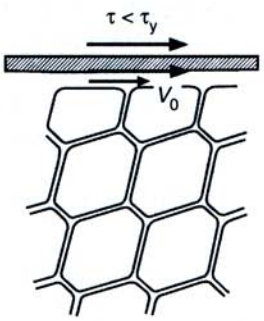

Fig. 6.15 *If the boundary bubbles slide with respect to the confining solid wall (relative velocity V_0), viscous friction appears in the wetting films, formed between the boundary bubbles and the wall surface. If the applied stress is lower than the foam yield stress, $\tau < \tau_y$, the foam is deformed elastically, without bubble rearrangements occurring. In contrast, when $\tau > \tau_y$, the foam also flows and the actual shear rate inside the foam depends on the wall-slip velocity, V_0.*

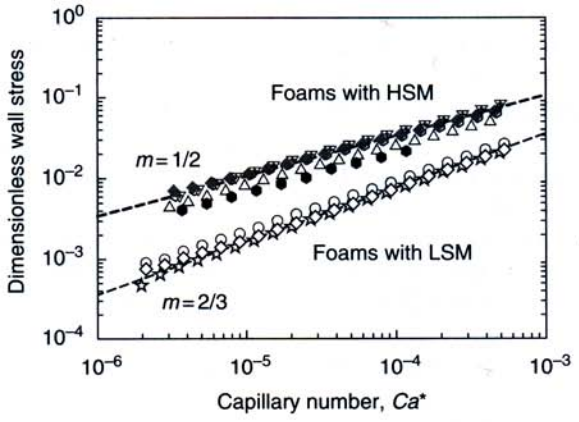

Fig. 6.16 *Dimensionless foam-wall friction stress, $\tau_w/(\sigma/R_{32})$, versus capillary number, $Ca^* = \mu V_0/\sigma$. The foams were prepared from different surfactant solutions whose viscosity was varied between 1 and 11 mPa.s by adding glycerol. In the various foams studied, the mean bubble radius varies between 100 and 300 μm, and the surface tension varies between 22 and 30 mN/m. The lines are drawn as guides to the eye with slopes corresponding to the indicated flow index,* m. *The air volume fraction is $\Phi = 0.90 \pm 0.01$.*

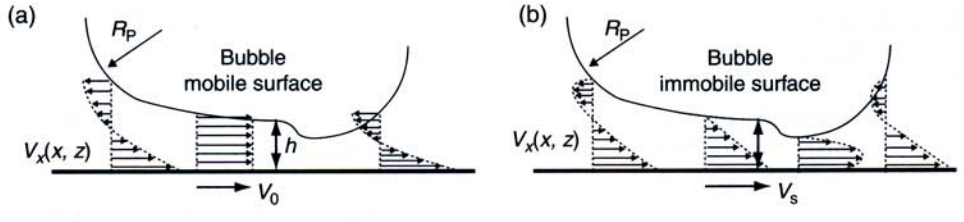

Fig. 6.17 *Schematic presentation of the zone of bubble–wall contact with the profile of the fluid velocity [17]. (a) In the case of tangentially mobile bubble surface, there is no velocity gradient in the wetting film, so that the bubble–wall friction originates in the meniscus zones around the film only. (b) In the case of tangentially immobile bubble surface, the friction occurs in both zones – of the film and in the surrounding meniscus regions. The theoretical models show that the friction in meniscus regions scales as $(Ca^*)^{2/3}$ for both mobile and immobile bubble surfaces, whereas the friction in the film region scales as $(Ca^*)^{1/2}$ (for immobile surface) [16, 17, 104, 105, 109].*

comparison with the foam-wall viscous stress. As illustrated in Fig. 6.16, the experimental results obtained with many different foam systems merge around two master lines, depending on the surface modulus of the foaming solutions: (i) systems with LSM give power-law index $m \approx 2/3$; (ii) systems with HSM give $m \approx 1/2$ [16–18, 54].

Several detailed theoretical models of the viscous friction between bubbles and smooth solid wall have been proposed [5, 16, 17, 104–109]. All of them are based on calculations of the fluid velocity profile in the wetting films, formed in the bubble–wall contact zone; see Fig. 6.17. In these calculations, a 'non-slip' boundary condition is used for the liquid flow at the surface of the solid wall, whereas different boundary conditions are considered

for the gas–liquid interface. For bubbles with tangentially mobile surfaces (those with LSM) one can assume a stress-free boundary condition, which results in a plug flow of the liquid inside the wetting films (i.e. flow without velocity gradient; see Fig. 6.17(a)). In contrast, solutions with HSM give bubbles with tangentially immobile surfaces; the usual non-slip boundary condition for the liquid flow can be applied and a velocity profile with a gradient is established in the wetting films (Fig. 6.17(b)). Once this velocity profile has been calculated, one can determine the resulting viscous stresses acting on the wall surface, τ_w [16, 17]. In most theoretical models, the numerical calculations are made for idealized, infinitely long cylindrical bubbles (2D bubbles) [5, 16, 17, 104–106]. In [16, 17] it is shown how the results for such model 2D bubbles could be extended to estimate τ_w for real 3D bubbles in foam slipping on a solid wall.

The theoretical models predict $\tau_w \propto (Ca^*)^{2/3}$ for the systems, in which the bubble–wall friction is dominated by the viscous stress in the curved menisci regions surrounding the wetting film [104, 105,109]. In contrast, $\tau_w \propto (Ca^*)^{1/2}$ is predicted for bubbles in which the bubble–wall friction is dominated by the viscous stress inside the wetting film, which is possible only if the bubble surface is tangentially immobile [16, 17]. These predictions are in good agreement with the experimental results [14–16]: the solutions with high surface modulus yield bubbles with tangentially immobile surface and $m \approx 1/2$, whereas solutions with low surface modulus lead to bubbles with tangentially mobile surface and $m \approx 2/3$ is measured; see Fig. 6.16.

It is worth mentioning that the surfactants that give mobile bubble surfaces in the foam–wall experiments were shown to behave as with immobile bubble surfaces in the inside-foam friction experiments [53, 110, 111]. Most probably, the reason for this non-trivial result is the qualitatively different dynamics of the bubbles and of the respective thin films in the two types of experiments. In the foam–wall friction experiments, the bubbles have stationary shape and the films have constant radius and thickness at given velocity of the wall. In contrast, the foam films between colliding bubbles in sheared foams have a limited lifetime, and continuously change their thickness and radius during this lifetime; see Fig. 4 in ref. [52]. Therefore, the viscous stresses exerted on the film surfaces, and the mass-transfer of surfactant towards/from the bubble surface, are qualitatively different in both types of experiments – steady state configuration is realized in the foam–wall friction experiments, whereas oscillations of the film and bubble surface areas are realized in sheared foams, with a frequency $\approx \dot{\gamma}$. Further model experiments with single bubbles or more detailed theoretical models, accounting for the dynamics of surfactant adsorption, could be very useful in clarifying this issue.

6.8 Conclusions

In recent years, significant progress towards a physical understanding of the multi-scale processes that govern the mechanical properties of liquid foams has been made. It has been demonstrated that foam rheology is controlled by a coupling between elastic and viscous effects: surface tension forces give rise to an elastic mechanical response, depending on bubble deformations, whereas viscous friction inside the films and Plateau channels, and/or in the surfactant adsorption layers, leads to viscous dissipation of energy.

Depending on the choice of surfactants, shear rate and foam ageing (bubble coarsening), one among several possible mechanisms of dissipation may prevail. To rationalize this complexity, it is necessary to identify experimentally the dominant physico-chemical processes at the scale of the bubbles and foam films, and to define adequate theoretical models.

The dependencies of foam viscosity, elasticity and yield stress on the bubble size, surface tension, solution viscosity and coarsening rate have been established experimentally and explained theoretically. The respective scaling laws have been used to describe conveniently a large variety of experimental data in terms of appropriate dimensionless quantities. This approach has provided much insight about the strong effects of the visco-elastic surface modulus of the foaming solution on several phenomena related to foam rheology – foam–wall friction, bulk viscous stress in flowing foam, and energy dissipation during fast visco-elastic relaxations. In addition, the influence of foam ageing (via bubble coarsening) on foam rheology has been clarified.

Many interesting questions in the field of foam rheology are still open and call for further investigation. What local mechanisms and macroscopic laws govern the flow of very wet or very dry foams? How can physico-chemical tools be used to control most efficiently the foam rheological properties? How deep is the analogy between foam, emulsion, paste and suspension rheology? A current direction of active research is the foam rheology in very short time scales. Sound propagation in foams [112], the mechanical impact of solid objects on foams [113] and blast mitigation by foams [114] all fall into this category. Another active field of research is the coupling between foam structure and flow. Examples are bubble break-up induced by shear flow [53], and the coupling between osmotic pressure and shear flow [2], called also 'dilatancy'. This non-exhaustive list of open questions clearly demonstrates how attractive this area currently is for fundamental research studies, with important practical implications.

Abbreviations

2D, 3D	two dimensional and three dimensional, respectively
CAPB	cocoamidopropyl betaine (amphoteric surfactant)
DWS	diffusing wave spectroscopy
HSM	high surface modulus
LAOS	large amplitude oscillation
LSM	low surface modulus
MRI	magnetic resonance imaging
SLES	sodium lauryl-trioxyethylene sulfate (anionic surfactant)

Acknowledgement

The authors are grateful for the support of this study to the bilateral research program 'Rila-4', funded by the French foundation 'EGIDE' and the National Science Fund of Bulgaria (project no. 202).

References

[1] R.K. Prud'homme and S.A. Khan (eds). *Foams: Theory, Measurements, and Applications,* Surfactant Science Series, Vol. 57. Marcel Dekker, New York, 1996.

[2] D. Weaire and S. Hutzler. *The Physics of Foams*. Oxford University Press, Oxford, 2001.

[3] D. Exerowa and P.M. Kruglyakov. *Foams and Foam Films: Theory, Experiment, Application*. Elsevier, Amsterdam, 1998.

[4] H.M. Princen. The structure, mechanics, and rheology of concentrated emulsions and fluid foams. In *Encyclopedia of Emulsion Technology*, J. Sjöblom (ed.). Marcel Dekker, New York, 2001.

[5] G.J. Hirasaki and J.B. Lawson. Mechanisms of foam flow in porous media: apparent viscosity in smooth capillaries. *Soc. Petroleum Eng. J.*, **25**: 176, 1985.

[6] D.A. Edwards, D.T. Wasan and H. Brenner. *Interfacial Transport Processes and Rheology*. Butterworth-Heinemann, Boston, 1991.

[7] A.M. Kraynik. Foam flows. *Ann. Rev. Fluid Mech.*, **20**: 325, 1988.

[8] D. Weaire. The rheology of foam. *Curr. Opin. Coll. Interface Sci.*, **13**: 171, 2008.

[9] D. Weaire and W. Drenckhan. Structure and dynamics of confined foams: A review of recent progress. *Adv. Coll. Interface Sci.*, **137**: 20, 2008.

[10] D. Weaire and S. Hutzler. Foam as a complex system. *J. Phys: Condens. Matter*, **21**: 474227, 2009.

[11] D. Weaire, J.D. Barry and S. Hutzler. The continuum theory of shear localization in two-dimensional foam. *J. Phys: Condens. Matter*, **22**: 193101, 2010.

[12] R. Höhler and S. Cohen-Addad. Rheology of liquid foam. *J. Phys: Condens. Matter*, **17**: R1041, 2005.

[13] D. Langevin. Aqueous foams: A field of investigation at the Frontier between chemistry and physics. *ChemPhysChem*, **9**: 510, 2008.

[14] N. Denkov, S. Tcholakova, K. Golemanov, K.P. Ananthpadmanabhan and A. Lips. Role of surfactant type and bubble surface mobility in foam rheology. *Soft Matter*, **7**: 3389, 2009.

[15] H.M. Princen. Rheology of foams and highly concentrated emulsions. II. Experimental study of the yield stress and wall effects for concentrated oil-in-water emulsions. *J. Coll. Interface Sci.*, **105**: 150, 1985.

[16] N.D. Denkov, V. Subraminian, D. Gurovich and A. Lips. Wall slip and viscous dissipation in sheared foams: Effect of surface mobility. *Coll. Surf. A*, **263**: 129, 2005.

[17] N.D. Denkov, S. Tcholakova, K. Golemanov, V. Subramanian and A. Lips. Foam–wall friction: Effect of air volume fraction for tangentially immobile bubble surface. *Coll. Surf. A*, **282/283**: 329, 2006.

[18] S. Marze, D. Langevin and A. Saint-Jalmes. Aqueous foam slip and shear regimes determined by rheometry and multiple light scattering. *J. Rheol.*, **52**: 1091, 2008.

[19] I. Cantat, N. Kern and R. Delannay. Dissipation in foam flowing through narrow channels. *Europhysics Lett.*, **65**: 726, 2004.

[20] C. Raufaste, A. Foulon and B. Dollet. Dissipation in quasi-two-dimensional flowing foams. *Phys. Fluids*, **21**: 053102, 2009.

[21] F. Rouyer, S. Cohen-Addad, M. Vignes-Adler and R. Höhler. Dynamics of yielding observed in a three-dimensional aqueous dry foam. *Phys. Rev. E*, **67**: 021405–7, 2003.

[22] P. Coussot and G. Ovarlez. Physical origin of shear-banding in jammed systems. *Europhys. J. E*, **33**: 183, 2010.

[23] G. Katgert and M. Van Hecke. Jamming and geometry of two-dimensional foams. *Europhys. Lett.*, **92**: 34002, 2010.

[24] P. Schall and M. Van Hecke. Shear bands in matter with granularity. *Annual Rev. Fluid Mech.*, **42**: 67, 2010.

[25] M. Dennin. Discontinuous jamming transitions in soft materials: Coexistence of flowing and jammed states. *J. Phys: Condens. Matter*, **20**: 283103, 2008.

[26] N.D. Denkov, S. Tcholakova, K. Golemanov and A. Lips. Jamming in sheared foams and emulsions, explained by critical instability of the films between neighbouring bubbles and drops. *Phys. Rev. Lett.*, **103**: 118302, 2009.

[27] S. Meeker, R.T. Bonnecaze and M. Cloitre. Slip and flow in pastes of soft particles: direct observations and rheology. *J. Rheol.*, **48**: 1295, 2004.
[28] J.R. Seth, M. Cloitre and R.T. Bonnecaze. Influence of short-range forces on wall-slip in microgel pastes. *J. Rheol.*, **52**: 1241, 2008.
[29] U. Seifert. Hydrodynamic lift on bound vesicles. *Phys. Rev. Lett.*, **83**: 876, 1999.
[30] H.M. Princen. Rheology of foams and highly concentrated emulsions: I. Elastic properties and yield stress of a cylindrical model system. *J. Coll. Interface Sci.*, **91**: 160, 1983.
[31] H.M. Princen and A.D. Kiss. Rheology of foams and highly concentrated emulsions: IV. An experimental study of the shear viscosity and yield stress of concentrated emulsions. *J. Coll. Interface Sci.*, **128**: 176, 1989.
[32] R. Soller and S.A. Koehler. Rheology of steady-state draining foams. *Phys. Rev. Lett.*, **100**: 208301, 2008.
[33] G. Ovarlez, S. Rodts, A. Ragouilliaux, P. Coussot, J. Goyon and A. Colin. Wide-gap Couette flows of dense emulsions: local concentration measurements, and comparison between macroscopic and local constitutive law measurements through magnetic resonance imaging. *Rhys. Rev. E*, **78**: 036307, 2008.
[34] C. Enzendorfer, R.A. Harris, P. Valko, M.J. Economides, P.A. Fokker and D.D. Davies. Pipe viscometry of foams. *J. Rheol.*, **39**: 345, 1995.
[35] G. Ovarlez, K. Krishan and S. Cohen-Addad. Investigation of shear banding in three-dimensional foams. *Europhys. Lett.* **91**: 68005, 2010.
[36] A.D. Gopal and D.J. Durian. Nonlinear bubble dynamics in a slowly driven foam. *Phys. Rev. Lett.*, **75**: 2610, 1995.
[37] A.D. Gopal and D.J. Durian. Shear-induced 'melting' of an aqueous foam. *J. Colloid Interface Sci.*, **213**: 169, 1999.
[38] R. Höhler, S. Cohen-Addad and H. Hoballah. Periodic nonlinear bubble motion in aqueous foam under oscillating shear strain. *Phys. Rev. Lett.*, **79**: 1154, 1997.
[39] M. Durand and H.A. Stone. Relaxation time of the topological T1 process in a two-dimensional foam. *Phys. Rev. Lett.*, **97**: 226101, 2006.
[40] J. Lauridsen, G. Chanan and M. Dennin. Velocity profiles in slowly sheared bubble rafts. *Phys. Rev. Lett.*, **93**: 018303, 2004.
[41] C. Gilbreth, S. Sullivan and M. Dennin. Flow transitions in two-dimensional foams. *Phys. Rev. E*, **74**: 051406, 2006.
[42] G. Debregeas, H. Tabuteau and J.-M di Meglio. Deformation and flow of a two-dimensional foam under continuous shear. *Phys. Rev. Lett.*, **87**: 178305, 2001.
[43] B. Dollet and F. Graner. Two-dimensional flow of foam around a circular obstacle: local measurements of elasticity, plasticity and flow. *J. Fluid Mech.*, **585**: 181, 2007.
[44] B. Dollet, M. Aubouy and F. Graner. Anti-inertial lift in foams: a signature of the elasticity of complex fluids. *Phys. Rev. Lett.*, **95**: 168303, 2005.
[45] C. Raufaste, S.J. Cox, P. Marmottant and F. Graner. Discrete rearranging disordered patterns: Prediction of elastic and plastic behaviour, and application to two-dimensional foams. *Phys. Rev.* E, **81**: 031404, 2010.
[46] G. Katgert, M.E. Möbius and M. van Hecke. Rate dependence and role of disorder in linearly sheared two-dimensional foams. *Phys. Rev. Lett.*, **101**: 058301, 2008.
[47] M.E. Möbius, G. Katgert and Martin van Hecke. Relaxation and flow in linearly sheared two-dimensional foams. *Europhys. Lett*, **90**: 44003, 2010.
[48] A.-L. Biance, S. Cohen-Addad and R. Höhler. Topological transition dynamics in a strained bubble cluster. *Soft Matter*, **5**: 4672, 2009.
[49] S. Hutzler, M. Saadatfar, A. van der Net, D. Weaire and S.J. Cox. The dynamics of a topological change in a system of soap films. *Coll. Surf. A*, **323**: 123, 2008.
[50] S. Besson and G. Debrégeas. Statics and dynamics of adhesion between two soap bubbles. *European Phys. J. E*, **24**: 109, 2007.
[51] N.D. Denkov, S. Tcholakova, K. Golemanov, K.P. Ananthapadmanabhan and A. Lips. Viscous friction in foams and concentrated emulsions under steady shear. *Phys. Rev. Lett.*, **100**: 138301, 2008.
[52] S. Tcholakova, N.D. Denkov, K. Golemanov, K.P. Ananthapadmanabhan and A. Lips. Theoretical model of viscous friction inside steadily sheared foams and concentrated emulsions. *Phys. Rev. E*, **78**: 011405, 2008.

[53] K. Golemanov, S. Tcholakova, N.D. Denkov, K.P. Ananthapadmanabhan and A. Lips. Breakup of bubbles and drops in steadily sheared foams and concentrated emulsions. *Phys. Rev. E*, **78**: 051405, 2008.
[54] K. Golemanov, N.D. Denkov, S. Tcholakova, M. Vethamuthu and A. Lips. Surfactant mixtures for control of bubble surface mobility in foam studies. *Langmuir*, **24**: 9956, 2008.
[55] D.M.A. Buzza, C.-Y.D. Lu and M.E. Cates. Linear shear rheology of incompressible foams. *J. Physique II France*, **5**: 37, 1995.
[56] K. Krishan, A. Helal, R. Höhler and S. Cohen-Addad. Fast relaxations in foam. *Phys. Rev. E*, **82**: 011405, 2010.
[57] S. Marze, R.M. Guillermic and A. Saint-Jalmes. Oscillatory rheology of aqueous foams: surfactant, liquid fraction, experimental protocol and aging effects. *Soft Matter*, **5**: 1937, 2009.
[58] L.W. Schwartz and H.M. Princen. A theory of extensional viscosity for flowing foams and concentrated emulsions. *J. Coll. Interface Sci.*, **118**: 201, 1987.
[59] D.A. Reinelt and A.M. Kraynik. Viscous effects in the rheology of foams and concentrated emulsions. *J. Coll. Interface Sci.*, **132**: 491, 1989.
[60] E. Janiaud, D. Weaire and S. Hutzler. Two-dimensional foam rheology with viscous drag. *Phys. Rev. Lett.*, **97**: 038302, 2006.
[61] V.J. Langlois, S. Hutzler and D. Weaire. Rheological properties of the soft-disk model of two-dimensional foams. *Phys. Rev. E*, **78**: 021401, 2008.
[62] D. Weaire, S. Hutzler, V.J. Langlois and R.J. Clancy. Velocity dependence of shear localisation in a 2D foam. *Philos. Mag. Lett.*, **88**: 387, 2008.
[63] D.J. Durian. Foam mechanics at the bubble scale. *Phys. Rev. Lett.*, **75**: 4780, 1995.
[64] D.J. Durian. Bubble-scale model of foam mechanics: Melting nonlinear behaviour, and avalanches. *Phys. Rev. E*, **55**: 1739, 1997.
[65] D. Stamenovic. A model of foam elasticity based upon the laws of Plateau. *J. Colloid Interface Sci.*, **145**: 255, 1991.
[66] R. Höhler, S. Cohen-Addad and V. Labiausse. A constitutive equation describing the nonlinear elastic response of aqueous foams and concentrated emulsions. *J. Rheol.*, **48**: 679, 2004.
[67] A.J. Liu, S. Ramaswamy, TG. Mason, H. Gang and D.A. Weitz. Anomalous viscous loss in emulsions. *Phys. Rev. Lett.*, **76**: 3017, 1996.
[68] G. Picard, A. Ajdari, F. Lequeux and L. Bocquet. Elastic consequences of a single plastic event: A step towards the microscopic modeling of the flow of yield stress fluids. *European Phys. J. E*, **15**: 371, 2004.
[69] http://www.susqu.edu/brakke/evolver.
[70] A.M. Kraynik, D.A. Reinelt and F.V. Swol. Structure of random monodisperse foam. *Phys. Rev. E*, **67**: 031403–11, 2003.
[71] A.M. Kraynik and D.A. Reinelt. Microrheology of random polydisperse foam. *Proc. XIVth Int. Congr. on Rheology*, 2004.
[72] S. Vincent-Bonnieu, R. Höhler and S. Cohen-Addad. Slow viscoelastic relaxation and aging in aqueous foam. *Europhysics Lett.*, **74**: 533, 2006.
[73] S. Vincent-Bonnieu. *Multiscale simulation and modelling of 2D foam rheology*. PhD thesis, 2006, University Marne-la-Vallée, Champs-sur-Marne.
[74] N. Kern, D. Weaire, A. Martin, S. Hutzler and S.J. Cox. Two-dimensional viscous froth model for foam dynamics. *Phys. Rev. E*, **70**: 041411, 2004.
[75] S.J. Cox. A viscous froth model for dry foams in the Surface Evolver. *Coll. Surf. A*, **263**: 81, 2005.
[76] P. Grassia, G. Montes-Atenas, L. Lue and T.E. Green. A foam film propagating in a confined geometry: analysis via the viscous froth model. *European Phys. J. E*, **25**: 39, 2008.
[77] I. Cantat, S. Cohen-Addad, F. Elias *et al. Les Mousses: Structure et Dynamique*. Belin, Paris, 2010.
[78] A.M. Kraynik and D.A. Reinelt. Linear elastic behaviour of dry soap foams. *J. Colloid Interface Sci.*, **181**: 511, 1996.
[79] K. Feitosa and D.J. Durian. Gas and liquid transport in steady-state aqueous foam. *European Phys. J. E*, **26**: 309, 2008.
[80] M. van Hecke. Topical review: Jamming of soft particles: geometry, mechanics, scaling and isostaticity. *J. Phys.: Condens. Matter*, **22**: 033101, 2010.

[81] A. Saint-Jalmes and D.J. Durian. Vanishing elasticity for wet foams: equivalence with emulsions and role of polydispersity. *J. Rheol.*, **43**: 1411, 1999.
[82] V. Labiausse, R. Hohler and S. Cohen-Addad. Shear induced normal stress differences in aqueous foams. *J. Rheol.*, **51**: 492, 2007.
[83] A.D. Gopal and D.J. Durian. Relaxing in foam. *Phys. Rev. Lett.*, **91**: 188303–4, 2003.
[84] C. Macosko. *Rheology, Principles, Measurements and Applications*. Wiley-VCH, New York, 1994.
[85] S. Cohen-Addad, R. Höhler and Y. Khidas. Origin of the slow linear viscoelastic response of aqueous foams. *Phys. Rev. Lett.*, **93**: 028302–4, 2004.
[86] D.J. Durian, D.A. Weitz and D.J. Pine. Scaling behaviour in shaving cream. *Phys. Rev. A*, **44**: R7902–5, 1991.
[87] S. Cohen-Addad and R. Höhler. Bubble dynamics relaxation in aqueous foam probed by multispeckle diffusing-wave spectroscopy. *Phys. Rev. Lett.*, **86**: 4700–3, 2001.
[88] S. Cohen-Addad, M. Krzan, R. Höhler and B. Herzhaft. Rigidity percolation in particle-laden foams. *Phys. Rev. Lett.*, **99**: 168001, 2007.
[89] S. Arditty, V. Schmitt, F. Lequeux and F. Leal-Calderon. Interfacial properties in solid-stabilized emulsions. *European Phys. J. B*, **44**: 381, 2005.
[90] R.G. Larson. *The Structure and Rheology of Complex Fluids*. Oxford University Press, New York, 1999.
[91] F. Rouyer, S. Cohen-Addad and R. Höhler. Is the yield stress of aqueous foam a well-defined quantity? *Colloids Surf. A*, **263**: 111, 2005.
[92] T.G. Mason, J. Bibette and D.A. Weitz. Yielding and flow of monodisperse emulsions. *J. Colloid Interface Sci.*, **179**: 439–48, 1996.
[93] F. Rouyer, S. Cohen-Addad, R. Höhler, P. Sollich and S.M. Fielding. The large amplitude oscillatory strain response of aqueous foam: Strain localization and full stress Fourier spectrum. *European Phys. J. E*, **27**: 309–21, 2008.
[94] S.A. Khan, C.A. Schnepper and R.C. Armstrong. Foam rheology: III. Measurement of shear flow properties. *J. Rheol.*, **32**: 69–92, 1988.
[95] B. Herzhaft, S. Kakadjian and M. Moan. Measurement and modeling of the flow behaviour of aqueous foams using a recirculating pipe rheometer. *Colloids Surf. A*, **263**: 153–64, 2005.
[96] P. Marmottant and F. Graner. An elastic, plastic, viscous model for slow shear of a liquid foam. *European Phys. J. E*, **23**: 337–47, 2007.
[97] S.M. Peker and S.S. Helvaci. *Solid–Liquid Two Phase Flow*. Elsevier, Amsterdam, 2008.
[98] L. Becu, S. Manneville and A. Colin. Yielding and flow in adhesive and nonadhesive concentrated emulsions. *Rhys. Rev. Lett.*, **96**: 138302, 2006.
[99] S. Rodts, J.C. Baudez and P. Coussot. From 'discrete' to 'continuum' flow in foams. *Europhys. Lett.*, **69**: 636, 2005.
[100] G. Katgert. PhD thesis, Leiden University, 2008.
[101] V. Carrier, S. Destouesse and A. Colin. Foam drainage: A film contribution? *Rhys Rev E*, **65**: 061404, 2002.
[102] S. Larmignat, D. Vanderpool, H.K. Lai and L. Pilon. Rheology of colloidal gas aphrons (microfoams). *Colloid Surf. A*, **322**: 199, 2008.
[103] J. Zhao, S. Pillai and L. Pilon. Rheology of microfoams made from ionic and non-ionic surfactant solutions. *Colloid Surf. A*, **348**: 93, 2009.
[104] F.P. Bretherton. The motion of long bubbles in tubes. *J. Fluid Mech.*, **10**: 166–188, 1961.
[105] L.W. Schwartz, H.M. Princen and A.D. Kiss. On the motion of bubbles in capillary tubes. *J. Fluid Mech.*, **172**: 259–75, 1986.
[106] J. Ratulowski and H.C. Chang. Marangoni effects of trace impurities on the motion of long gas bubbles in capillaries. *J. Fluid Mech.*, **210**: 303–28, 1990.
[107] H. Wong, C.J. Radke and S. Morris. Motion of long bubbles in polygonal capillaries. Part 1. Thin films. *J. Fluid Mech.*, **292**: 71, 1995.
[108] H. Wong, C.J. Radke and S. Morris. Motion of long bubbles in polygonal capillaries. Part 2. Drag, fluid pressure and fluid flow. *J. Fluid Mech.*, **292**: 95, 1995.
[109] A. Saugey, W. Drenkhan and D. Weaire. Wall slip of bubbles in foams. *Phys. Fluids*, **18**: 053101, 2006.
[110] A. Prins and F. van Voorst Vader. *Proc. 6th Int. Congr. Surf. Act. Subst. (Zurich)*, 1972, 441.

[111] J. Lucassen. *In Anionic Surfactants: Physical Chemistry of Surfactant Action*, Lucassen and E. H. Reynders (Eds). Dekker, New York, 1981; pp 11.
[112] M. Erpelding, R.M. Guillermic, B. Dollet, A. Saint-Jalmes and J. Crassous. Investigating acoustic-induced deformations in a foam using multiple light scattering. *Rhys. Rev. E*, **82**: 021409, 2010.
[113] A. Le Goff, L. Courbin, H.A. Stone and D. Quéré. Energy absorption in a bamboo foam. *Europhys. Lett.*, **84**: 36001, 2008.
[114] Britan, M. Liverts and G. Ben-Dor. Mitigation of sound waves by wet aqueous foams. *Colloid Surf. A*, **344**: 48, 2009.